https://doi.org/10.1016/j.buildenv.2020.106862

Effects of envelope features on wind flow and pollutant exposure in street canyons

Dongjin Cui[1], Xingdi Li[1], Yaxing Du*[2], Cheuk Ming Mak[3], Kenny Kwok[4]

[1]*School of Architecture and Urban Planning, Shenzhen University, China*
[2]*Department of Particulate Flow Modelling, Johannes Kepler University, Linz,*
[3]*Department of Building Services Engineering, The Hong Kong Polytechnic University, Hong Kong*
[4]*School of Civil Engineering, The University of Sydney, Australia*

*Corresponding author: Yaxing Du

Phone: +43 732 2468 6489 Fax: +43 732 2468 6462

Email: yaxing.du@gmail.com

Highlights

- Effects of different envelope features on pollutant exposure are investigated
- Intake fraction and daily pollutant exposure are used to quantify the exposure risk
- Envelope features increase the pollutant exposure risk for the leeward residents
- Envelope features reduce pollutant exposure risk of windward residents

Abstract

Traffic pollution has posed a serious threat to the health of near-road city residents and pedestrians, especially in high-density cities. However, the influences of envelope features, including balconies, overhangs and wing walls, on pollutant exposure to near road residents and pedestrians have not been fully understood. This paper investigates the effects of three commonly-used envelope features on wind flow and pollutant exposure to residents in street canyon with three different aspect ratios. The evaluation metrics of personal intake fraction and daily pollutant exposure are used to quantitatively assess the influences caused by different envelope features on healthy risk of near-road residents and pedestrians, alongside with wind flow pattern and pollutant distribution. The results show that these envelope features have increased the risk of pollutant exposure for the leeward side residents, while the risk of pollutant exposure for the windward side residents is reduced for most cases, in particular for the first floor. This observation is especially prominent when the canyon has the highest aspect ratio among the tested ratios, with the increased ratio of personal intake fraction reaching up to 540%. Moreover, the pollutant concentration is overall higher on leeward side of upstream building than that of windward side of downstream building. These findings can help urban planners and architects to build healthy and sustainable urban environment.

Keywords: *envelope features; pollutant exposure; CFD simulation; street canyon*

1. Introduction

Nowadays, the rapid development of urbanization has resulted in deteriorating air quality, especially in developing countries. Among many different pollutant sources in cities, traffic emission cannot be ignored and becomes one of major sources [1, 2]. Moreover, outdoor traffic pollutant can enter the interior via doors, windows, ventilation systems and building cracks [3]~~[3, 4]~~. Therefore, city residents who lives near traffic roads and pedestrians are more likely

to be exposed to large amount of vehicular pollutant, which calls for special attention and further investigation.

Improvement of urban ventilation can be considered as one of effective methods to reduce the pollutant exposure of near-road residents. In a long street canyon which length ratio (canyon length/width, $LR=L/W$) is larger than 7, the key factor that affects the urban ventilation rate is aspect ratio (building height/street width, $AR=H/W$) when the approaching wind is perpendicular to the street canyon and the building heights are uniform [4]. Additionally, building packing density [5], building height variations (uneven urban layouts) [6], lift-up building designs [7-9], overall urban forms (street shape) [10] and ambient wind directions [4, 11] also affect urban ventilation. In urban microclimate studies, two-dimensional (2D) street canyon is widely investigated since it is a typical representative of urban spatial components that can be viewed as a reduction to complex urban forms for long street canyon [12-14]. Hang et al [2] investigated the pollutant exposure in 2D street canyon for different aspect ratios (H/W=1-6), and found that the pollutant exposure is much larger when the street canyon presents two main recirculation (H/W=4-6) than that of one main recirculation (H/W=1-2). At the same time, high-density cities usually consist of deep street canyons with various envelope features [15]. These bring up the necessity to investigate the pollutant exposure in deep street canyons, especially with commonly-used envelope features, e.g., balconies, overhangs and wing walls.

Envelope features, which are indispensable in cities, can have a significant impact on urban natural ventilation [16], thermal comfort [17], and indoor air quality [18]. Ai and Mak [19] used computational fluid dynamics (CFD) to explore how balconies affect indoor ventilation performance in terms of mass flow rate and airflow velocity on the working plane. Their results showed that the presence of balconies could significantly change the airflow pattern within and around buildings. Latter, they [15] examined the impact of eight envelope features on the single-

sided natural ventilation performance of buildings and concluded that a horizontal feature located in the middle of an opening could enhance indoor natural ventilation. With regard to the envelop feature of overhang, Park et al. [20] reported that it could slightly decrease the ventilation rates of the leeward and side rooms while enhance the ventilation rate in the windward room for various wind speeds. The numerical study of the ventilation performance of wing walls performed by Mak et al. [21] indicated that wing walls can improve the mean indoor air speed and air change per hour for various wind directions and wind speeds. Consequently, they concluded that wing walls can improve indoor natural ventilation. Murea and Mele [22] studied the influence of balcony on pollutant dispersion inside a deep street canyon (aspect ratio of 3), and revealed that the envelop feature of balcony played an important role on the pollutant dispersion. By consulting the relevant literature [20-22], the authors find that most previous studies have focused on how envelope features affect near-wall flow pattern. Contrary to this, the effects of envelope feature on street canyon flow structure dispersion have not yet received detailed investigations.

Furthermore, previous studies have paid attention on the influences of urban geometry on city ventilation and pollutant dispersion [5, 10]. However, the pollutant exposure is also essential to residents living in near-road buildings, but it has not yet obtained the attention they deserve. The intake fraction (*IF*) is the representative fraction of pollutants inhaled, on average, by each person based on the total emitted pollutants. *IF* of 1ppm (one per million, 10^{-6}) means that if 1kg of pollutants are emitted by vehicles, 1 mg of them will be inhaled by the population. It has been used to assess the traffic-related pollutant exposure of different age populations in urban micro-environment [23]. Habilomatis and Chaloulakou [24] evaluated the population exposure to vehicle emitted ultrafine particle in a real street canyon using *IF*. The quantification of evaluation helps to test multiple emission source, e.g. vehicles fueled by diesel and gasoline.

The daily pollutant exposure is the extent of people being exposed to pollutant within one day [2]. Thus, the above pollutant exposure indexes are adopted in this paper.

This paper focuses on high-resolution 2D CFD simulation of wind flow structure and pollutant dispersion in a street canyon. The exposure risk of near-road residents is quantified by personal intake fraction(*P_IF*) and daily pollutant exposure. The pollutant concentration of the window area on the building façade is used to evaluate the exposure risk, which have also been employed by other studies [23]. The objective of this paper has two-folds: first, the influences of three commonly-used envelop features, e.g., wing walls, overhang and balcony, on wind flow and pollutant dispersion inside street canyon are thoroughly investigated. Second, the exposure risk of near-road residents and pedestrians are quantitatively assessed, which provides scientific foundations on city planning for building a healthy and sustainable city.

The rest of this paper is organized in the following order: Section 2 introduces the definition of *P_IF* and daily pollutant exposure index. Section 3 presents the CFD methodologies and validation results. Section 4 gives model descriptions of the studied cases. Section 5 presents results and analysis and concludes the paper.

2. Pollutant exposure indexes

2.1 Pollutant intake fraction (*IF*) and personal intake fraction (*P_IF*)

The pollutant intake fraction (*IF*) is defined as the fraction of total pollutant emission quantity (e.g., vehicle emitted exhausts) inhaled by the population. For one specific city area, the *IF* can be expressed as following:

$$IF = \sum_i^N \sum_j^M P_i B_{i,j} \Delta t_{i,j} C_j / q \qquad (1)$$

here, *i*, *N* denote the age group of exposed population, *i* is the *i*th age group and totally *N* number of age group is considered. P_i is the exposed population number for *i*th age group. *j*, *M* are the

micro-climate conditions, and two different conditions are considered in this study, e.g., pedestrian level and indoor area. B_j is the mean volumetric breathing rate, m^3/s. Δt_j is the length of stay. C_j is the pollutant concentration at specific location, i.e. pedestrian level or window inside the canyon and q is the total emission quantity.

To obtain the independence of population density, the personal intake fraction is defined following the *IF* by considering the demographic structure as follows:

$$P\_IF = IF / \sum_i^N P_i \qquad (2)$$

In this research, we divide the whole population into three age groups (N=3) according to the population census data [25] (Fig. 1): children (p=1), adults (p=2) and elders (p=3). Four micro-environments (M=4) are considered [26], and they are indoors at home, other indoor locations, near vehicles, other outdoor locations away from vehicles. Breathing rate, time activity patterns and population ratio for each age group in Shenzhen are referred to the literature [25, 26].

Table 1. Breathing rate for various age groups and different micro-environments.

Breathing rate Br(m^3/day)	**Indoor at home** (j=1)	**Other indoor locations** (j=2)	**Near Vehicle** (j=3)	**Other outdoor locations** (j=4)
Children	12.5	14	14	18.7
Adults	13.8	15.5	15.5	20.5
Elderly	13.1	14.8	14.8	19.5

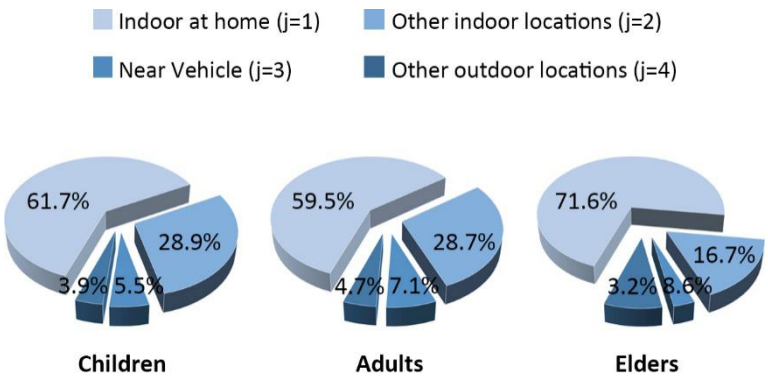

(a)

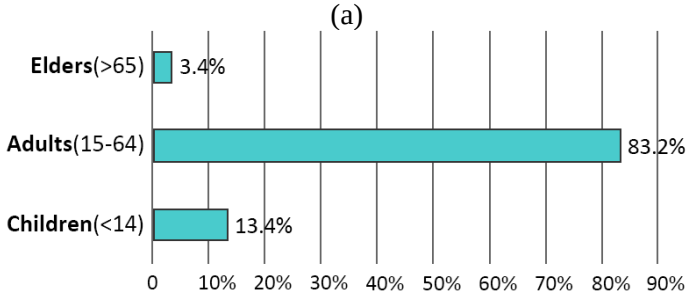

(b)

Fig. 1. (a) Time activity patterns for different age groups and micro-environments; and (b) demographic structure in Shenzhen, China.

2.2 Daily pollutant exposure index

The definition of daily pollutant exposure is the extent of people being exposed to pollutant within one day, as written below as it shown in Eq. (2):

$$E_d = \sum_j^M E_{d,j} = \sum_j^M \sum_i^N C_{i,j}\, t_{ij} \qquad (3)$$

here, $C_{i,j}$ denotes for the pollutant concentration, t_{ij} is the time spent for different activities, as illustrated in Fig. 1 and Table 1. Similar to the definition of P_IF, i, N denote the age group of exposed population and j, M denote the micro-climate conditions.

3. Model validation

3.1 Wind flow validation

To conduct the measurement of the flow field within a street canyon, Li et al. [27] performed a water tunnel ($L_T \times W_T \times H_T$ = 10 m × 0.3 m × 0.5m) experiment. The experiment investigated two types of street canyons of AR (H_B/W_S) equal to 1.0 and 2.0, which consisted of eight and ten selfsame building models ($L_B \times W_B \times H_B$ = 0.3 m × 0.1 m × 0.1 m). The water flow reached the street canyons perpendicularly (Fig. 2b). All canyons have the same height: H_B = 0.1 m. The two groups of experiments applied under the same water depth of 0.4 m. The Reynolds number was 12,000, calculated from the reference water speed (U_{ref} = 1.8 m/s) in free stream at

z = 0.3 m and the building height was 0.1 m. Roughness elements on the tunnel ground were not considered. A two-color Laser Doppler anemometer (LDA) was used to measure velocity components in the stream-wise and vertical directions, and the measurements were conducted along three vertical lines and two horizontal lines on the vertical center-plane (y = 0) (see Fig. 2a).

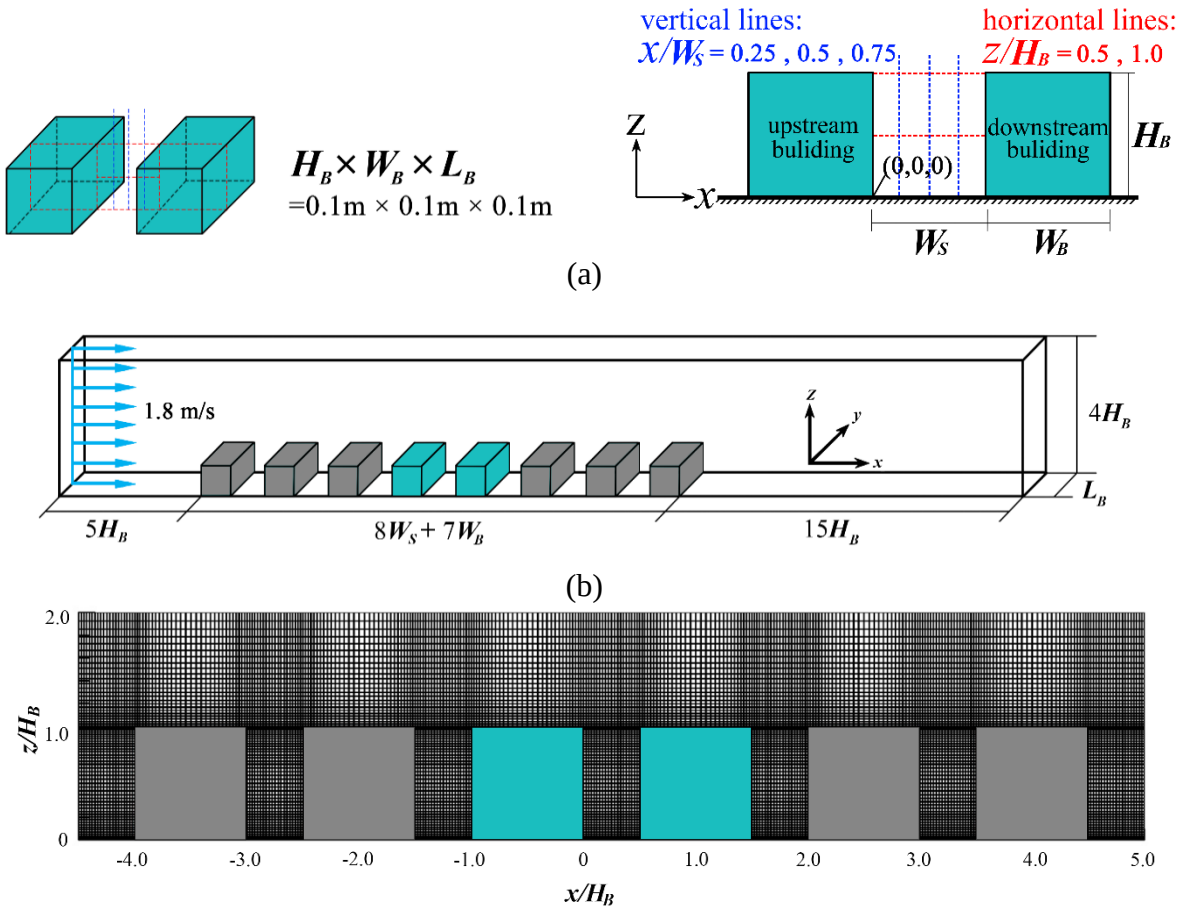

Fig. 2. (a) Canyon geometry and measurement lines; (b) computational domain; and (c) grid arrangement on vertical center-plane (AR = 2).

The CFD simulations shared the same geometry of canyon models with the water tunnel experiments (see Fig. 2a-b) performed by Li et al [27]. The computational domain was set by following the existing best practice guidelines for CFD simulation of urban aerodynamics [28, 29], and the domain had the same height and lateral length of the experiments. The whole computational domain was decomposed by structured hexahedral cells (see Fig. 2c). Based on a grid sensitivity test, two grids with 3,168,000 and 2,880,000 cells in total, were used to the

cases of AR = 1.0 and 2.0, separately. The y^+ values at first cells, whose height was 1.665 mm, vary from 0 to 15, and the average value was 5.3. The highest y^+ value only occurred at the top corners of the windward facades because of the relatively high wind velocity.

The inlet of the computational domain shared the same uniform wind speed of 1.8 m/s with the experiments. The inflow adopted a turbulence intensity of 5% and a turbulent length scale of 0.35 m, based on the sensitivity analysis of turbulence characteristics of the inflow against experimental data of velocity field. Pressure outlet with zero static pressure was defined for the domain outlet. At the lateral sides and the top of the domain, zero normal velocity and zero normal gradients of all variables were specified. No-slip walls were adopted for the domain ground and the building surfaces.

The CFD simulations were performed using ANSYS Fluent 15.0.0. The flow fields were predicted by applying the steady-state two-equation Reynolds-Averaged Navier-Stokes (RANS) model, namely Re-Normalization Group (RNG) $k-\varepsilon$ model [30]. RNG $k-\varepsilon$ model was chosen because it performed well in predicting flow in and around buildings [31]. As for the near-wall regions, the two-layer model was adopted. SIMPLEC algorithm was applied to couple the pressure and momentum equations, and the second-order upwind scheme is used in the discretization scheme. Convergence didn't occur until all scaled residuals were below 10^{-5} and the average wind speeds at important locations inside the street canyon were constant for over 50 iterations.

The velocity components in x direction obtained from CFD simulation and experiment are compared in Fig. 3. The comparison vertical and horizontal lines on the vertical center-plane located in the target street canyon are illustrated in Fig. 2a. It can be seen from Fig. 3 that the average relative deviation is less than 10% for all the comparison lines. The relative deviation of 10% indicates that the CFD predictions agree well with the experimental data. This degree

of discrepancies between experimental data and simulated results were also reported in [27] as well.

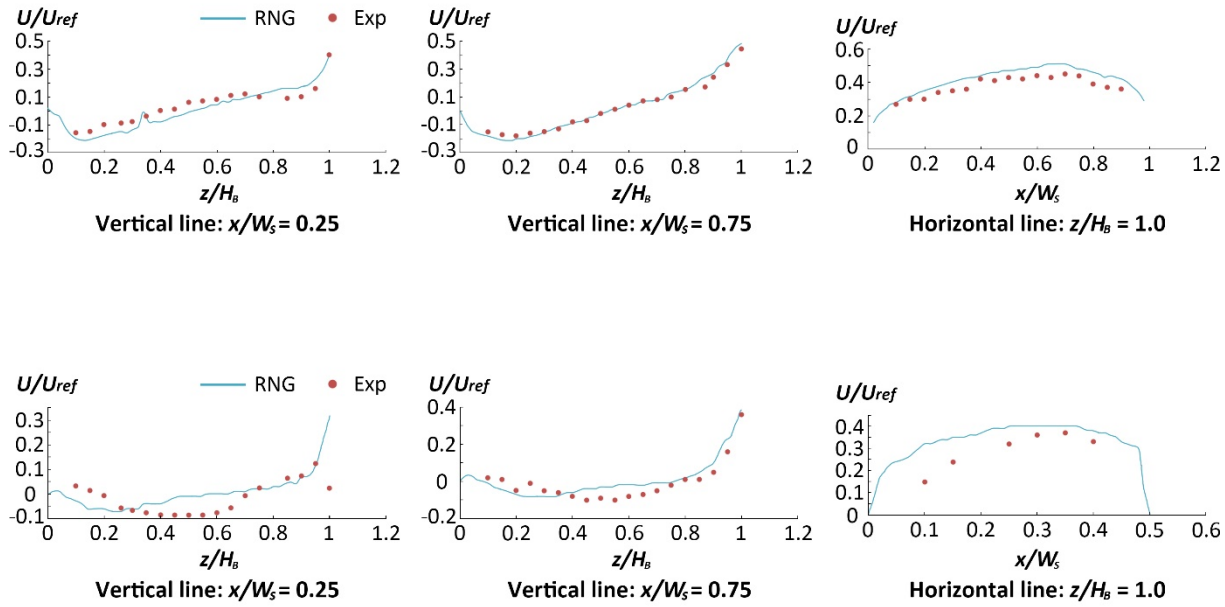

Fig. 3. Velocity components in x and z directions along two horizontal lines and four vertical lines on the vertical center-plane of the target street canyon.

3.2 Pollutant dispersion validation

To validate the pollutant dispersion, the wind tunnel measurements conducted by Li and Meroney [32] is used here. The cubic building ($L_B \times W_B \times H_B$ = 0.05 m × 0.05 m × 0.05 m) was immersed in a neutrally stratified turbulent atmospheric boundary layer. The incident wind speed at building height was 3.3 m/s, and the wind profile followed the power law with exponent of 0.19. The incident wind flow was perpendicular to the windward face of the cubic building. The pollutant was released from the central of building rooftop, which was a mixture of helium and air. The emission speed was 0.627 m/s. Some measurements of pollutant concentration were conducted in the building wake, as shown in Fig. 4. More detailed information can be found in the publication of Li and Meroney [32]. The above mentioned turbulence models, e.g., RNG $k - \varepsilon$ model, and the numerical setting are adopted here for the pollutant dispersion modelling. In addition, the species transport equation (6) was solved. The

non-dimensional concentration ratio (C/C_0) is used here, where C is the local concentration and C_0 is the reference concentration at emission. The comparison results between CFD simulation and wind tunnel test results of three vertical lines are shown in Fig. 4. It can be seen that the CFD simulation results agree well with the experimental data. Most of the deviations between CFD results and experimental data fall within 10%. On the whole, the CFD method applied in this paper including the turbulence model used here (namely, RNG $k-\varepsilon$ model) and numerical settings can satisfactorily predict the flow field in the street canyon and the pollutant dispersion around buildings. Thus, these are adopted for the rest of the paper.

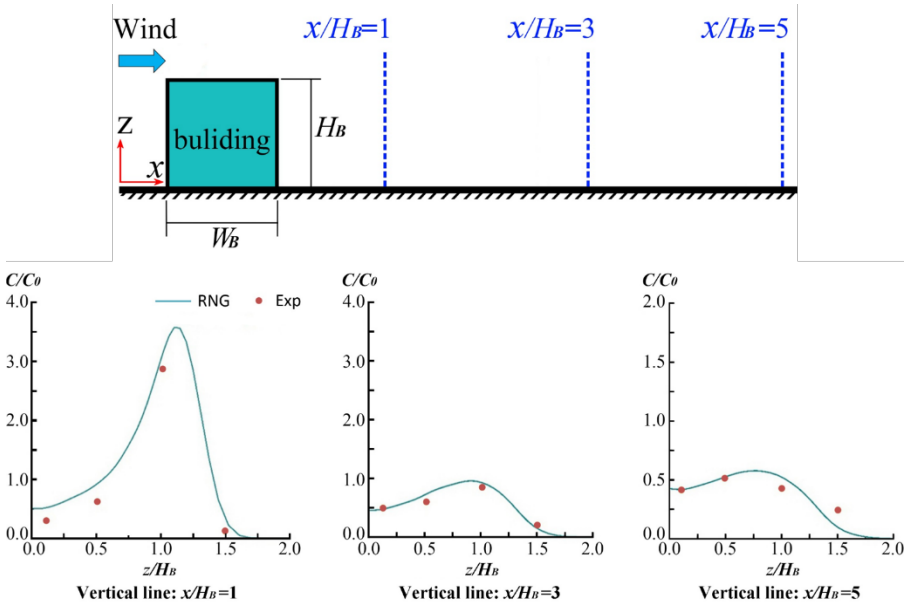

Fig. 4. Validation of CFD simulation by comparison with wind tunnel data.

4. Model description

4.1 Computational geometry

The computational domain of two-dimensional (2D) full-scale street canyon is described in Fig. 5a. Two selfsame canyons are set in the upstream region of the target street canyon while one in the downstream (Fig. 5a), for purpose of explicitly reproducing roughness elements. It should be noted that two methods are available to cope with the approaching flows to the target canyon

model from the domain inlet. First, to get horizontally homogeneous atmospheric boundary layer (*ABL*), many previous studies assigned specific settings of the roughness height K_S and roughness constant C_S at the upstream and downstream ground of the CFD domain [33]. Second, certain numbers of building units can be used as roughness elements and to help develop an urban boundary layer, which are fixed in the upstream and downstream ground [34, 35]. In this investigation, the second method are used. Additionally, in order to reproduce a reasonable boundary, some previous literatures employed two or three upstream street canyons as the explicit roughness elements of the target street [23, 35], while others only treat the target street canyon as the modeling domain [24]. In this study, the two upstream canyons are set according to previous studies [23] to obtain a reasonable boundary.

To discover the influences of envelope features on wind flow structure and pollutant dispersion investigated in this study, the street canyon without any envelope feature (basic case) is schematically shown in Fig. 5, together with its symbols of physical dimensions. As shown in Fig. 5, the height of canyon (H_1) is 12 m, and each story is set as 3 m with one window considered in prototype. L is length of slice domain, here L is set as 6 m in prototype as recommend in previous researches [2, 12]. This is set in consideration of dimension of window width (4 m in prototype), and symmetrical boundary conditions are used the lateral side of street canyon to avoid lateral flow interaction. The distance between the computational domain roof and canyon roof (H_2) is three times the canyon height. Three different canyon aspect ratios (H_1/W = 1, 2 and 3) were considered. The width (L_O) and height (H_O) of the windows are 4 m and 2 m respectively, which is located in the center of the building façade on each floor. The pedestrian level is defined as 1.5m in this study. For the purpose of quantitative investigation of different envelope features, the basic case is modified by introducing various envelope features. The layouts of the envelope feature in the deep canyon and their corresponding physical dimension are illustrated in Fig. 6 and Table 2. Totally three types of physical models

(envelope features) are considered, e.g., balcony (Fig. 6a), overhang (Fig. 6b) and wing walls (Fig. 6c). It's worth mentioning that the height of balcony (H_B) is 1.5m and all features are 1 meter out from the facade in prototype, namely W_B, W_V and W_g are equal to 1m. The detailed information of these studied models is listed in Table 2.

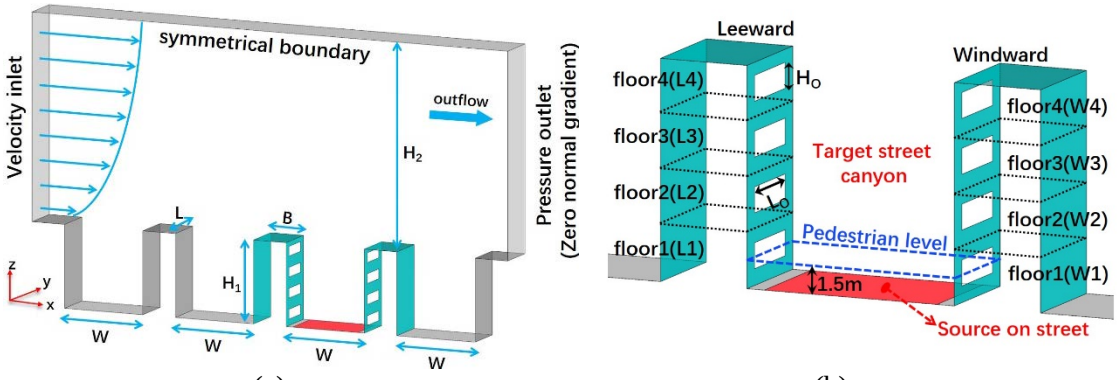

(a) (b)

Fig. 5. Sketch of basic deep canyon arrangement.

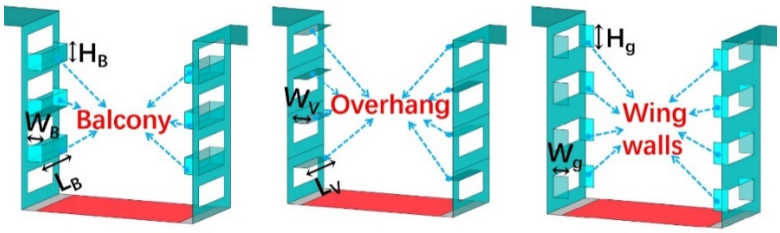

(a) (b) (c)

Fig. 6. Sketches of deep canyon with various envelope features.

Table 2. Summary of physical parameters for deep canyons models

Envelope features setting	Case Name (H=12m, W=12m, 6m, 4m)	
Basic case (Flat facade)	**N[*H*/*W*]**	**N(*H*/*W*=1)** **N(*H*/*W*=2)** **N(H/W=3)**
Balcony	**BA[*H*/*W*]**	**BA(*H*/*W*=1)** **BA(*H*/*W*=2)** **BA(*H*/*W*=3)**
Overhang	**OH[*H*/*W*]**	**OH(*H*/*W*=1)** **OH(*H*/*W*=2)** **OH(*H*/*W*=3)**
Wing walls	**WA[*H*/*W*]**	**WA(*H*/*W*=1)** **WA(*H*/*W*=2)** **WA(*H*/*W*=3)**

Simulations based on a reduced-scale model must obey Reynolds (*Re*) number independence [36]. To save computational cost while achieve Reynolds number independence, a 1:15 reduced-scale model is applied. The *Re* number calculated at building height is high enough to acquire *Re* number independence in this investigation, which is close to 2.4×10^5 [36]. Also, the *Re* numbers calculated near the envelop features are all over 1×10^4.

To make sure numerical solutions are independent, based on the cell number, we performed grid sensitivity test for the basic case of $AR = 1$. A coarse grid, a medium grid and a fine grid are constructed separately. The first grid is reset using a factor of nearly 1.5, to acquire the medium and fine grid. Overall, all these three grids are high-resolution ($y^+ < 10.0$) for meshing and resolving the near-wall boundary layer. The grid information on a vertical plane across a building of the street canyon is shown in Fig. 7 a-b. As shown in Fig. 7a-b, the computational domain is constructed using hexahedral cells. The minimum size for coarse grid, medium grid and fine grid is 0.006 m, 0.004 m and 0.0027 m, respectively. Meanwhile, the mesh stretching ratios are kept under 1.08 for both cases. This results in 1.07 million, 8.71 million and 10.21 million cells for basic case (with flat building facades). In addition, for a certain *AR* value, cases containing envelope features apply more cells than the basic case, which can be seen in Fig. 7b. The results of mesh sensitivity test along the center line of the target canyon are shown in Fig. 7b. The comparison shows that the mean deviation between the predictions by the medium grids and those by the fine grid is 8.0%, indicating that these two grids are very close. Contrary to this, the deviation between the medium and coarse grids reaches 37.9%. This comparison denotes that the medium grid is fine enough to ensure the accuracy of the simulations, which is eventually selected in this investigation. Other cases of $AR = 2, 3$, adopt the same grid settings as those of the basic case of $AR = 1$.

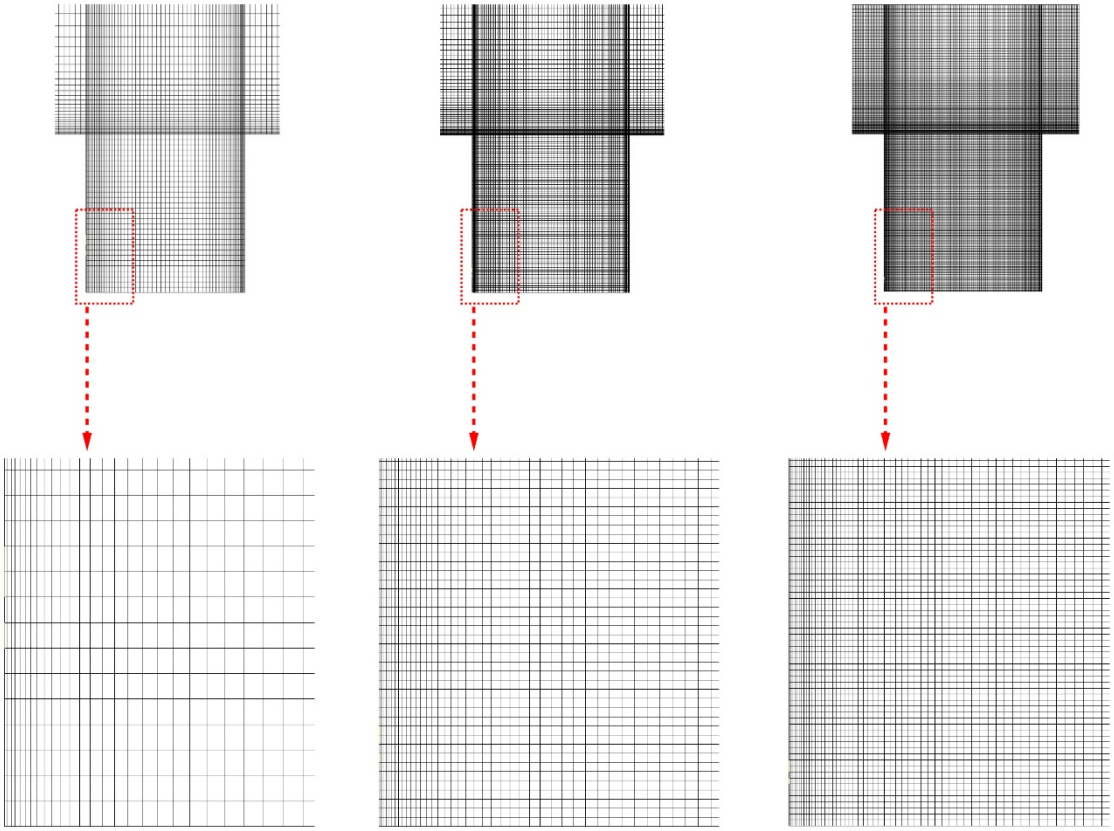

(a)

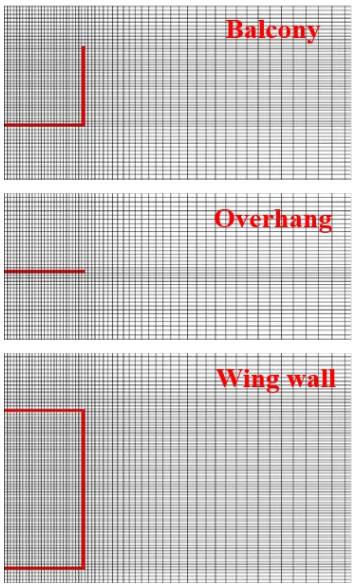
Balcony
Overhang
Wing wall

(b)

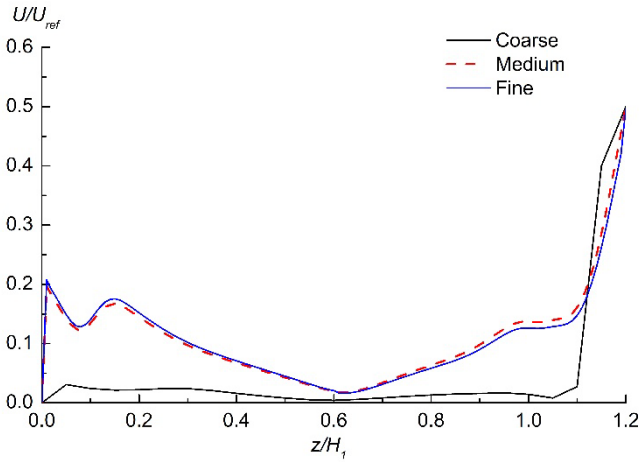
U/U_ref
0.6
0.5
0.4
0.3
0.2
0.1
0.0
0.0
0.2
0.4
0.6
0.8
1.0
1.2
z/H_1
Coarse
Medium
Fine

(c)

Figure. 7. (a) Detailed mesh information for all the cases; (b) Mesh around envelop features; and (c) Sensitivity test results.

4.2 Boundary conditions and numerical settings

In this study, we adopt the power-law velocity profile for the domain inlet according to Eqs. (3)-(5), the reference velocity (U_{ref}) is U_{ref} = 4m/s, at the height of z_{ref} = 2 H_1 and z_{ref} = 24m. H_1 is the height of building, and the velocity at building height is 3.48 m/s according to Eq. (4). The power law exponent (α) is 0.2, which corresponds to the Terrain Category 2 stipulated in Standards Australia/Standards New Zealand, AS.NZS 1170.2 [37]. The turbulence intensity at reference height is 10%. The empirical constant C_μ in Eq. (4) is 0.085. l is the character length, which is the building height. The domain outlet, lateral sides, ceiling and building surfaces share the same boundary conditions as the validation in Section 3. Meanwhile, the numerical settings are also same as the ones in Section 3.

$$U = U_{H_1}\left(\frac{z}{z_{H_1}}\right)^{\alpha} \quad (4)$$

$$k = \frac{3}{2}(uI)^2 \quad (5)$$

$$\varepsilon = C_\mu k^{3/2}/l \quad (6)$$

4.3 Species transport modeling

This investigation used carbon monoxide (CO) as the vehicular pollutant in the target street canyon. As is described in Fig. 5b, there is only one ground-level CO source in all cases. All cases share the same CO release rate.

The governing equation of time-averaged concentration is shown in Eq. (6):

$$\frac{\partial(C\,u_j)}{\partial x_j} = -\frac{\partial}{\partial x_j}(D_m + D_t)\frac{\partial C}{\partial x_j} + S \quad (6)$$

where u_j represents the time-averaged velocity component. C is the time-averaged concentration (kg/m^3). D_m and D_t ($D_t = \mu_t / Sc_t$) are the molecular and turbulent diffusivity of CO, respectively. Sc_t is the turbulent Schmidt number, equals to 0.7. S is pollutant emission rate, which is set as 1.25×10^{-6} kg/m^3/s on the basis of the realistic CO release rate in high traffic flux cities street.

5. Results and discussion

5.1 Wind flow pattern in deep canyon

This section focuses on the influences of various envelope features on the flow patterns in street canyons. The velocity ratio is defined by local velocity magnitude to reference velocity magnitude.

5.1.1 Wind flow pattern for *H/W*=1

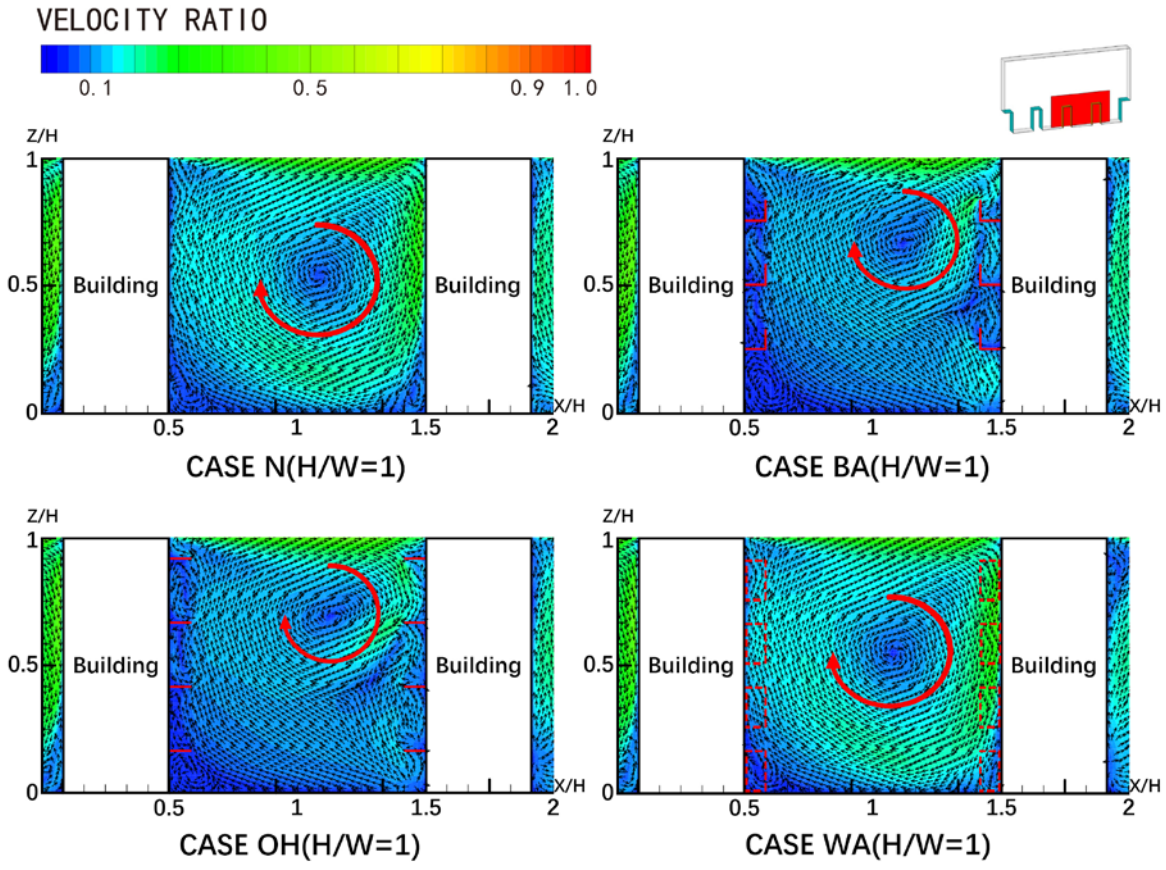

Fig. 8 Wind flow patterns for *H/W*=1.

Fig. 8 presents the results of wind flow patterns inside street canyon and around different envelope features for the aspect ratio of 1 (*H/W*=1). Generally, a clear primary recirculation is formed within the street canyon for different envelope features, and the flow velocity in the windward face of the downstream building is evidently higher than that in the leeward face of the upstream building. Compared to the basic case, the recirculation center moves up and close to the downstream building when the balcony and overhang are used. The other distinction between the basic case and other cases with envelope features is that the flow stream in the basic case is replaced by small recirculation around the envelope features. For the balcony, the wind velocity within balcony area is lower in the leeward face of upstream building than that of windward face of downstream building, and the flow patterns are disorderly within the balcony area. For the overhang, at the fourth floor, a small anti-clock recirculation is formed within the overhang area in the leeward face of upstream building, while the flow pattern within the overhang area remains the same as the basic case for the windward face of downstream building. However, for other lower floors, the flow patterns within the overhang area are mostly upward. For the wing walls, the flow patterns are very similar to the basic case since the wing walls structures are parallel to the dominant wind flow inside the street canyon.

5.1.2 Wind flow pattern for *H/W*=2

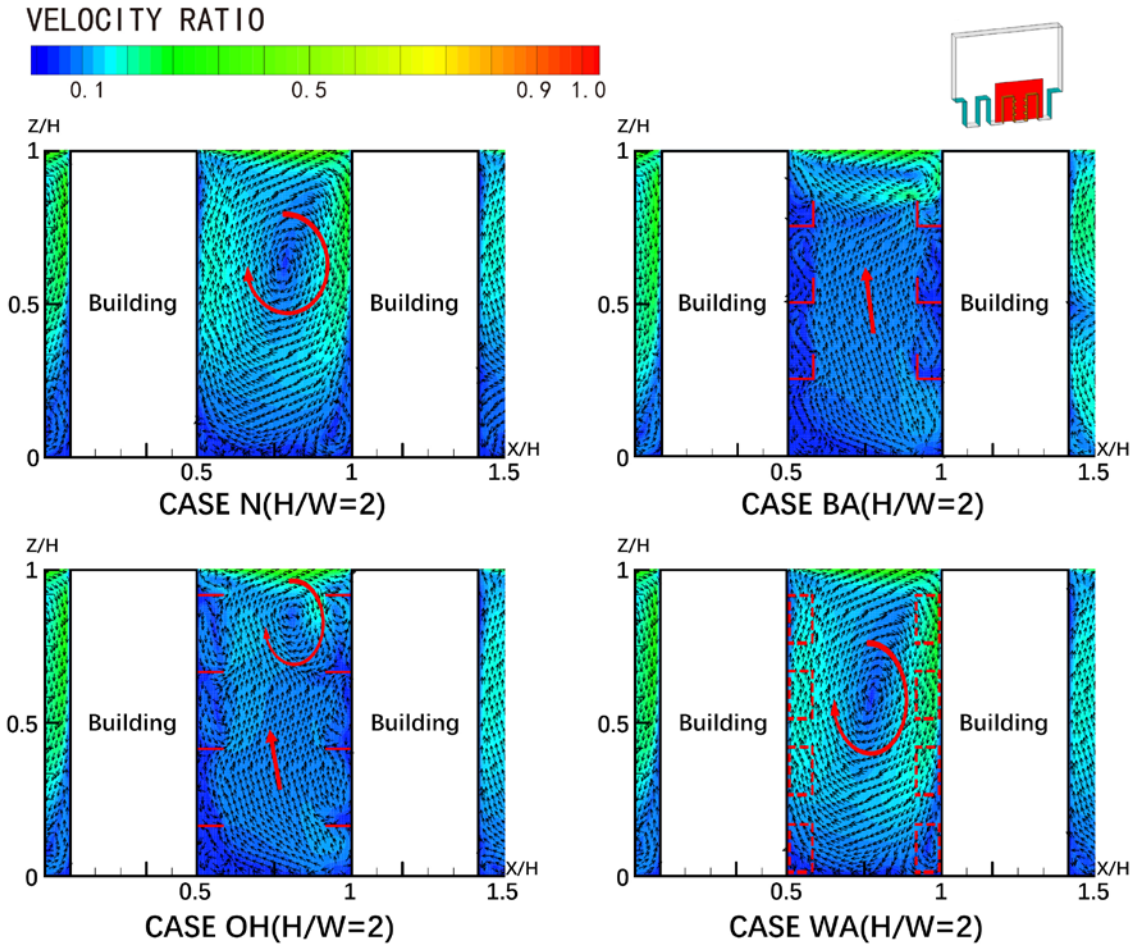

Fig. 9 Wind flow patterns for *H/W*=2.

The wind flow patterns inside street canyon and around the envelope features for the canyon aspect ratio of 2 are showed in Fig. 9. It can be seen that the center point of the primary recirculation is located in the upper part of the street canyon for the basic case. For the case with balcony, the primary recirculation disappears and a dominant upward flow appears. For the case with overhang, the flow is mainly upward in the lower part of street canyon and a small recirculation appears in the upper part of street canyon. However, a primary recirculation can be found in the case of wing wall and the center point is lower than that of the basic case. In general, the wind velocity in the lower part of the street canyon is smaller than that of the upper part of the street canyon. Compared to the other two envelope features (overhang and balcony), the wing walls experience higher wind velocity in both the leeward face of the upstream

building and the windward face of the downstream building. This is because the wing walls structures are parallel to the dominant wind recirculation in the street canyon and the Venturi effect inside the wing walls structure increases the wind velocity. Moreover, the wind velocities inside the overhang and balcony structure are much lower than that of basic case without any envelope features because of the horizontal airflow disturbance, especially near the windward face of downstream building.

5.1.3 Wind flow pattern for *H/W*=3

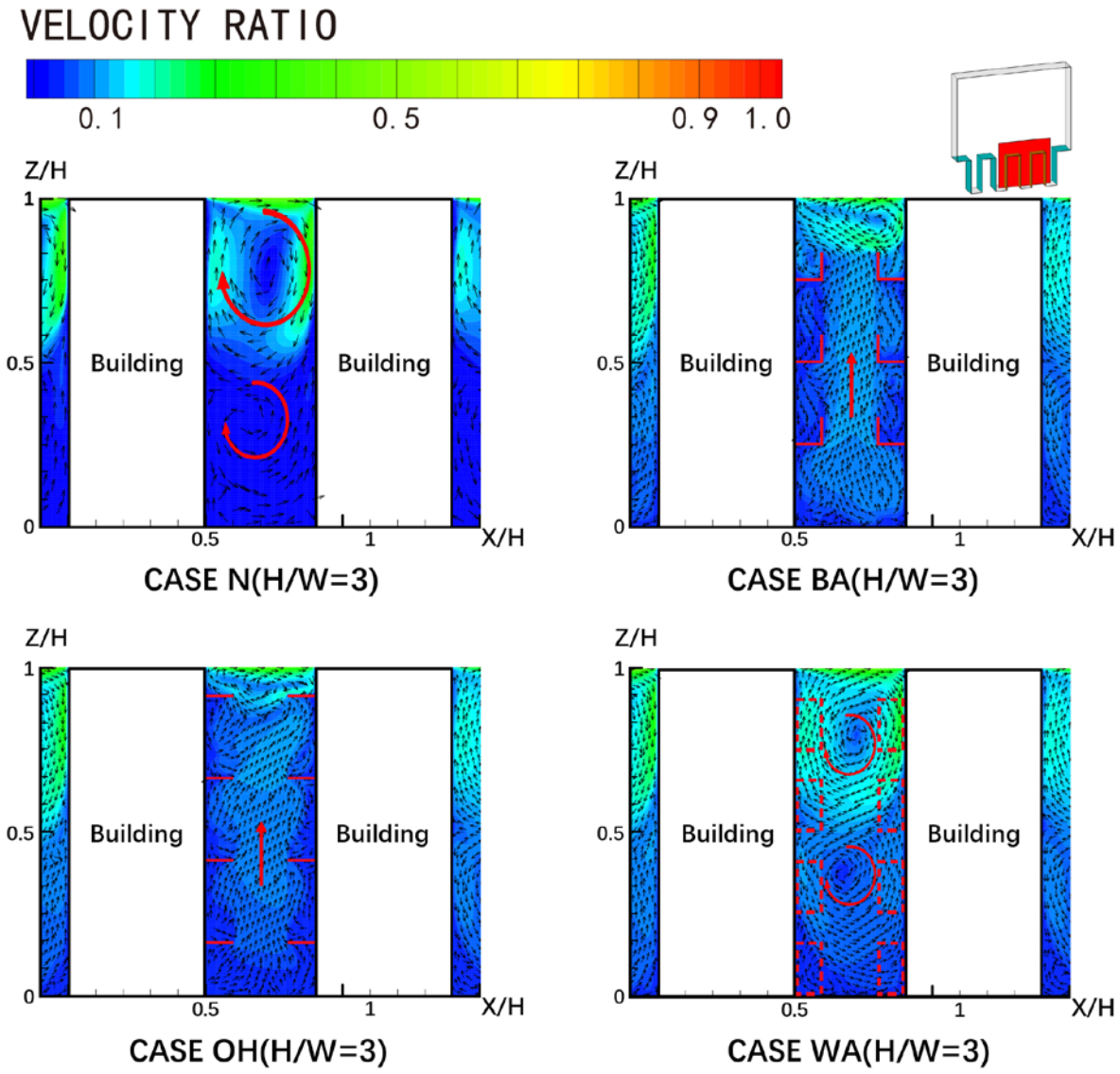

Fig. 10 Wind flow pattern for *H/W*=3.

Fig. 10 shows the wind flow patterns inside the street canyon and around the envelope features for the aspect ratio of 3. It can be observed that a second anti-clockwise recirculation is formed at the lower part of the street canyon for the basic case and wing wall case. The airflow at lower part of the street canyon does not coupled with the outside flow directly, which is also corresponds with the findings from He et al [23]. Similar to Fig. 9, a clear dominant upward flow can be found with the case of balcony, which is also the phenomenon for overhang case. Compared to the other two street canyons with lower aspect ratios, this street canyon has the lowest wind velocity in general (Fig. 10 vs Fig. 8-9). In particular, the bottom regions of street canyon have lower wind velocity than that of the upper region. It is interesting to find that the wind velocity of the street canyon bottom (first floor) is higher with envelop features than that of the basic case. This is especially prominent for the balcony cases due to its dominant upward flow inside the street canyon.

5.2 Pollutant distribution in deep canyon

The influences of different envelope feature on pollutant dispersion are presented in this section. To be clear, the pollutant is a line source and emits from the center of the canyon bottom surface, which represents vehicular pollutant. To presents the results in universal, the non-dimensional concentration ratio (C/C_0) is used to describe the concentration distribution. C is the local concentration and is C_0 the reference concentration at the source location, e.g. the center of the canyon bottom surface.

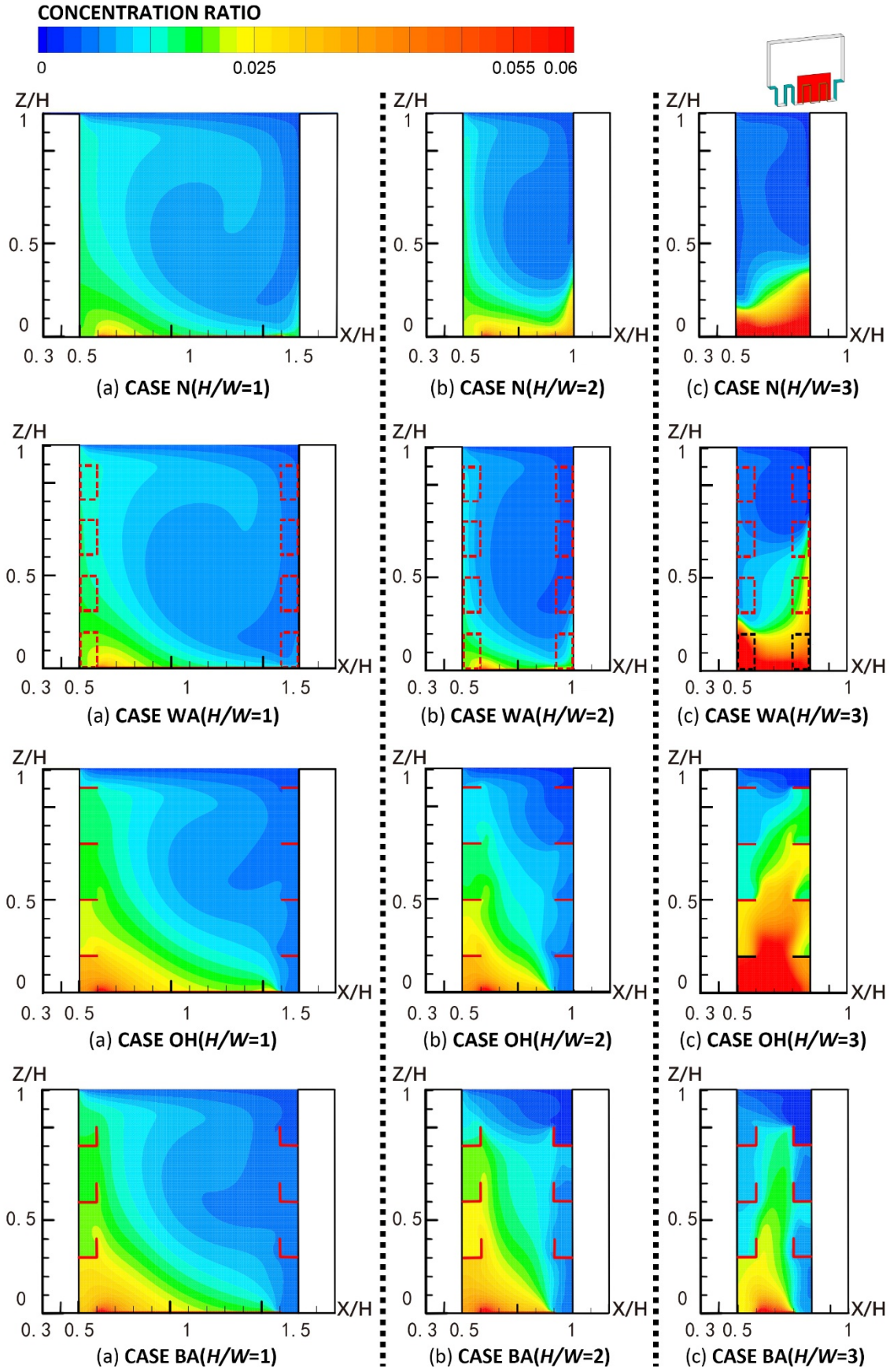

Fig. 11. Pollutant concentration for all the cases: (a) H/W=1; (b) H/W=2; (c) H/W=3.

Fig. 11 shows the pollutant concentration distribution for all cases with different aspect ratios. For the cases with aspect ratio of 1 or 2 (Fig. 11a-b), the pollutant concentration is much higher on leeward face of upstream building than that of windward face of downstream building. This is because of the primary wind flow inside the street canyon is a clockwise ~~vortex~~ recirculation, which carries the pollutants to the leeward face of the upstream building first and then to the windward face of downstream building. For basic case, the pollutant concentration at the bottom region of street canyon increases as the street aspect ratio become larger. This becomes more evident for the case with aspect ratio of 3, which can be attributed to the fact that the wind flow at the bottom region is decoupled from the wind flow in the upper part of the street canyon as explained in Section 5.1.

For wing wall envelop feature, the pollutant concentration on the windward face of the downstream building is relatively higher than that of the basic case when the aspect ratio is 3. In this case, the wing walls structure creates a "Venturi effect" for the pollutant dispersion. Overall, compared to the other envelope features (to be presented below), the wing walls has the least effect on the pollutant transportation. For overhang envelop feature, the pollutant concentration at the bottom region of street canyon significantly increases compared to the basic case, especially when the aspect ratio is 3. Moreover, when the aspect ratio is 1, the pollutant concentration on the leeward face of the upstream building and inside of the street canyon of Case OH and Case BA is higher than that of Case N and Case WA, especially at pedestrian level. For balcony envelop feature, the pollutant concentration pattern does not change too much compared to the basic case when the aspect ratio is 1. However, the pollutant concentration changes significantly when the street aspect ratio is 2 or 3. For the case with aspect ratio of 2, the pollutant concentration of the leeward face of upstream building is significantly increased, whereas the pollutant concentration inside the balcony on the windward face is decreased. Furthermore, the pollutant is dispersed to the upper regions inside the street

canyon due to the presence of balcony when the aspect ratio is 3. This is mainly because the upward flow pattern inside the street canyon due to the presence of balcony.

5.3 Personal intake fraction (*P_IF*) in deep canyon

The results of personal intake fraction for leeward windows of the upstream building are summarized in Table 3. The building under consideration is a typical residential building located in Shenzhen, and the population is viewed as equally distributed. The results in Table 3 are calculated from Equation (1-2), and the pollutant concentration from Section 5.2 is used here along with the statistical data from Table 1 and Fig. 1. The window position is taken as the condition of indoor at home, and the spatially averaged pollutant concentration of the window is used for the calculation of *P_IF* values. In general, the *P_IF* values increase as the aspect ratio increases, and the *P_IF* values decrease as the window is located farther away from the ground (bottom face of the street canyon). Compared to the basic cases, the *P_IF* values are mostly higher for each windows in leeward face of the upstream building when the envelop features are used. For the basic case, the windows on the first floor are very sensitive to the aspect ratio changes, and the *P_IF* values are doubled when the aspect ratio changes from 1 to 2, and 2 to 3, respectively. Besides, the *P_IF* values of L2, L3 and L4 decrease when the aspect ratio increases from 2 to 3 for the basic case. For the cases with balcony, the *P_IF* values for each windows (L1, L2, L3 and L4) have similar trend between the cases with aspect ratio 2 and 3. However, the *P_IF* values are remarkably smaller in case with aspect ratio of 1 than that of 2 or 3. For the cases with overhangs, *P_IF* values of all the windows increase as aspect ratio increases, which is also the case for the wing walls. Moreover, it is worth mentioning that the *P_IF* values of L1 for overhang and wing walls are significantly higher than the other cases because of the poor ventilation inside the bottom of the street canyon. This means that special

attention should be paid to the first floor window at leeward face of upstream building when the overhang or wing walls is used.

Table 3. Personal intake fraction (*P_IF*) for leeward face window in each case

		P_IF (unit: ppm)		
Cases	Windows	H/W=1	H/W=2	H/W=3
Basic	L1	306.2	819.1	1756.0
	L2	272.9	623.8	414.1
	L3	253.9	538.5	431.3
	L4	238.1	473.9	465.5
Balcony	L1	495.5	1440.2	1687.4
	L2	359.6	1020.4	1048.0
	L3	313.4	836.7	819.3
	L4	300.2	679.8	649.1
Overhang	L1	577.4	1395.2	4263.9
	L2	360.7	961.4	1794.0
	L3	307.1	726.6	1022.2
	L4	276.0	553.1	754.5
Wing walls	L1	322.3	888.7	6280.3
	L2	286.3	648.5	734.1
	L3	266.2	553.3	649.7
	L4	250.7	488.7	578.9

Table 4. Personal intake fraction (*P_IF*) for windward face window in each case

		P_IF (unit: ppm)		
Cases	Window	*H/W*=1	*H/W*=2	*H/W*=3
Basic	W1	210.8	1544.6	4165.6
	W2	101.4	654.3	1158.1
	W3	88.0	182.1	616.7
	W4	80.9	160.7	208.5
Balcony	W1	90.1	250.1	504.5
	W2	94.8	306.8	705.2
	W3	88.2	310.7	532.8
	W4	76.2	117.7	200.7
Overhang	W1	102.9	234.4	2271.2
	W2	110.5	323.4	2368.3
	W3	113.2	357.5	1959.8
	W4	88.3	194.4	1342.0
Wing walls	W1	154.1	767.9	3536.3
	W2	110.6	439.9	2312.0
	W3	85.4	162.1	1709.8
	W4	79.4	192.8	203.6

Table 4 summarized *P_IF* values for windward windows for these cases. It can be seen that the *P_IF* values increase as the canyon aspect ratio increases for all the cases, which is the same as presented in Table 3. In particular, the *P_IF* values of the all the windows at the windward of downstream building are significantly larger in cases with aspect ratio of 3 than that of 1 or 2. Nevertheless, the *P_IF* values increase as the aspect ratio increase is relatively stable for the cases with balcony compared to other envelop features. Unlike the results listed in Table 3, the influence of different envelop features on *P_IF* values of the windward window are mostly smaller than that of leeward windows. It should note that *P_IF* values of W1 and W2 in balcony cases is evidently smaller than that of the basic cases. This is mainly because of the upward flow is occurred inside the street canyon due to the presence of balcony.

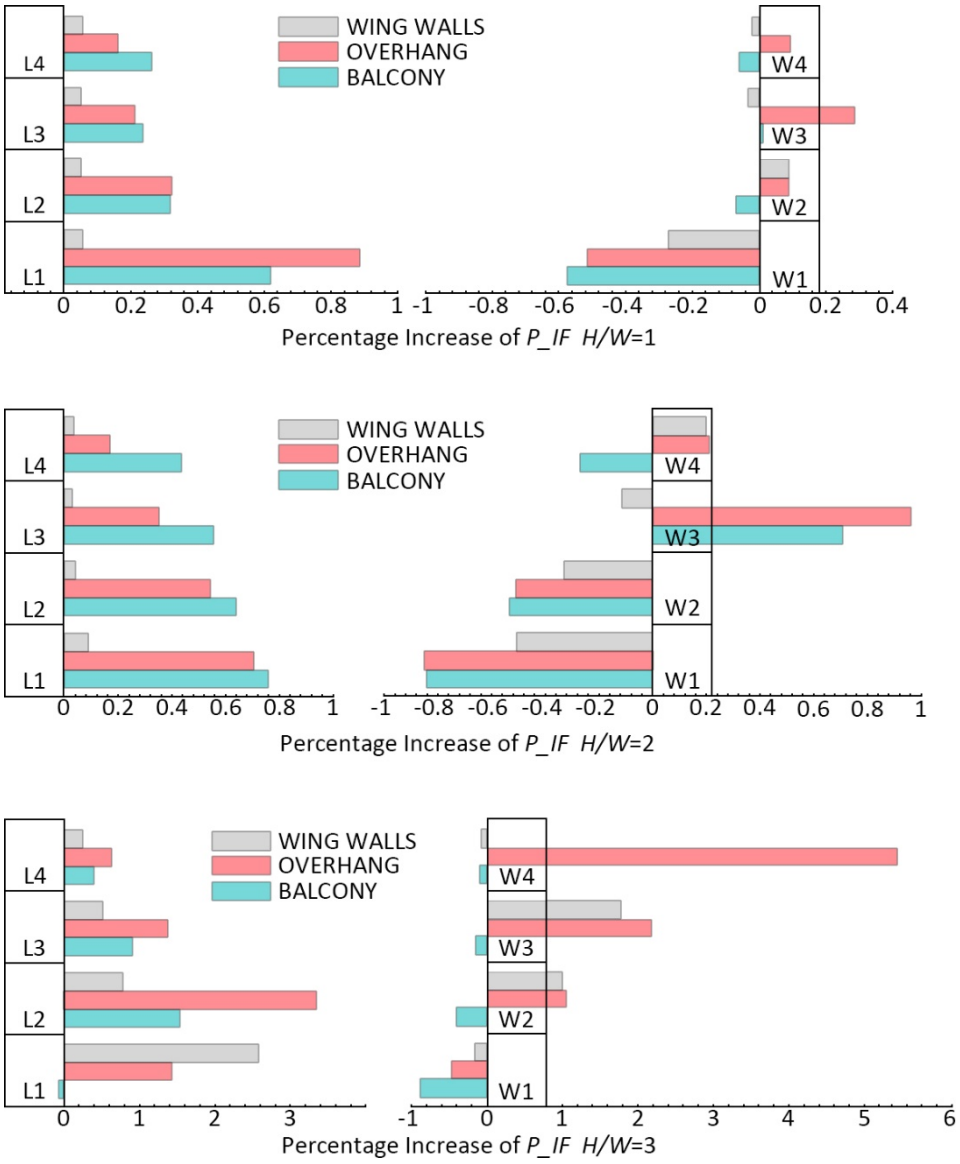

Fig. 12 *P_IF* change ratio between the basic case and different envelope features.

The differences of *P_IF* values between different envelop features and its corresponding basic cases are presented in Fig. 12. It is calculated by the difference of *P_IF* values between different envelop features and its corresponding basic cases to the *P_IF* values of corresponding basic cases. Compared with the basic case, the *P_IF* values generally increase on the leeward face of the upstream building, whereas the *P_IF* values decrease on the windward. It can be found that the magnitude of the change ratios caused by these envelop features all falls within 100% when the canyon aspect ratio is 1 or 2. However, the magnitude of the change ratios on the leeward face of the upstream building are mostly exceeds 100%, except for the highest floor (fourth

floor). Extreme values of *P_IF* change ratio (over 100%) on the windward windows occurs when the aspect ratio is 3 for wing walls and overhangs. This indicates that special care should be taken when the wing walls and overhangs are adopted in street canyon with aspect ratio of 3. The overhang envelop feature has the greatest influence on the *P_IF* values among these three envelop features, while the wing walls has the least impact on *P_IF* values. The magnitude of the influences caused by the balcony is mostly within 100%. The influence of wing walls is relatively subtle when the canyon aspect ratio is 1 or 2, while its influence becomes prominent when the canyon aspect ratio is 3.

5.4 Daily pollutant exposure in deep canyon

This subsection quantifies the influences of three envelope features on daily pollutant exposure (E_d). Table 5 listed the E_d values for the leeward window of the upstream building and Table 6 summarized the E_d values for the windward window of the downstream building. It can be seen that the E_d values decrease as the vertical height gets higher, which is the same as explained in Section 5.2. Generally, for the leeward window, the E_d values are higher when the building has balcony, overhang and wing-wall compared to that of the basic case. This means that these envelop features have increased the risk of pollutant exposure for the leeward residents. However, for the windward window, most of the E_d values are significantly smaller when the building has balcony, overhang and wing walls compared to that of the basic case. This is especially true for the windows on first floor, which are prone to be affected most by the pollutant emitted from the traffic on the road than the other higher floors.

Table 5. Daily pollutant exposure (E_d) for leeward face window in each cases

		E_d (unit: mg/m^3/day)		
Cases	Windows	*H/W*=1	*H/W*=2	*H/W*=3
Basic case	L1	331.0	354.2	379.7
	L2	295.1	269.7	89.5

	L3	274.5	232.9	93.2
	L4	257.4	204.9	100.6
Balcony	L1	535.7	622.8	364.8
	L2	388.8	441.3	226.6
	L3	338.9	361.8	177.1
	L4	324.6	294.0	140.3
Overhang	L1	624.2	603.4	922.0
	L2	390.0	415.7	387.9
	L3	332.0	314.2	221.0
	L4	298.4	239.2	163.16
Wing walls	L1	348.4	384.3	1358.0
	L2	309.6	280.4	158.7
	L3	287.8	239.3	140.4
	L4	271.0	211.3	125.1

Table 6. Daily pollutant exposure (E_d) for windward face window in each cases

		E_d (unit: mg/m^3/day)		
Cases	Window	*H/W*=1	*H/W*=2	*H/W*=3
Basic case	W1	227.9	667.9	900.7
	W2	109.7	282.9	250.4
	W3	95.1	78.7	133.3
	W4	87.4	69.5	45.1
Balcony	W1	97.4	108.1	109.1
	W2	102.5	132.6	152.5
	W3	95.4	134.3	115.2
	W4	82.4	50.9	43.4
Overhang	W1	111.3	101.3	491.1
	W2	119.5	139.8	512.1
	W3	122.4	154.6	423.7
	W4	95.5	84.1	290.1
Wing walls	W1	166.6	332.1	764.6
	W2	119.6	190.2	499.9
	W3	92.3	70.1	369.7
	W4	85.8	83.4	44.0

6. Discussion

This study is conducted for the long street canyon, which has a length ratio (canyon length/width) is larger than 7. However, the horizontal air flow cannot be neglected for small district with short street canyon (canyon length/width is smaller than 5). Thus, more complex geometry (e.g., 3D) should be used for small district simulation. The influences of envelop

feature on wind flow and pollutant exposure in short street canyon will be studied in future works.

It can be concluded from this study that the presence of these envelop features has greatly affected the wind flow structures and pollutant dispersion mechanisms inside the canyon, especially around the envelop features. Even though the current CFD models and numerical models have shown satisfactory results, further works still need to be conducted to find the effects of different numerical settings on simulation results around the envelop features, e.g., turbulence models (different Reynolds-averaged Navier-Stokes models, detached eddy simulation model and large eddy simulation model) and modeling constants. Further, the role of turbulent kinetic energy, convective and turbulent mass flux on the prediction accuracy of CFD simulations and dispersion mechanisms should also be studied in future work.

7. Conclusion

This paper focuses on investigating the influences of three commonly-used envelope features on wind flow, pollutant dispersion, personal intake fraction and daily pollutant exposure in street canyons with different aspect ratio. CFD technique was used to simulate the wind flow and pollutant dispersion after its validation against experimental data. The main findings are listed as follows:

i. The wind flow structure is changed greatly in near wall regions.
ii. The pollutant concentration is overall higher on the leeward façade of the upstream building than that of the windward façade of the downstream building.
iii. Generally, the pollutant concentration within the street canyon increases due to the presence of overhang and balcony envelop feature. The wing wall has least influence on pollutant concentration within the street canyon among the three envelop features.

iv. When the canyon aspect ratio is 3, the pollutant concentration at lower level (floor 1 and 2) is decreased due to the balcony presence.

v. The *P_IF* values increase as the canyon aspect ratio increases, and the *P_IF* values are smaller as the window location is farther away from the ground (pollutant source location).

vi. In general, the overhang envelope feature affects the *P_IF* values more than the other two envelope features, which is followed by balcony.

vii. These envelop features increase the *P_IF* values of the leeward windows of the upstream buildings, while reduce the *P_IF* values of the windward windows of the downstream buildings for most of the cases.

viii. For all the envelope features, on the change in *P_IF* values all falls within ±100% when the canyon aspect ratio is 1 or 2. However, these influences become very prominent when the canyon aspect ratio is 3, in which case of the change in *P_IF* value can be as high as +540%.

ix. Evidently, these envelope features increase the risk of pollution exposure for the leeward face residents, while the risk of pollutant exposure for the windward face residents decreases for most of cases, in particular for the lower floor.

The highlight of this work is that the personal intake fraction and daily pollutant exposure are adopted to quantify the influences of these building envelope features on health risk. These findings fill the knowledge gap between building design and pollution control strategies to assist city planners and architects to build healthy and sustainable cities.

Acknowledgement

The work described in this paper was supported by National Natural Science Foundation of China (grant no 51808342) and Natural Science Foundation of Shenzhen (JCYJ20180305125219726).

References

[1] J. Fenger, Urban air quality, Atmos. Environ. 33(29) (1999) 4877-4900.
[2] J. Hang, Z.W. Luo, X.M. Wang, L.J. He, B.M. Wang, W. Zhu, The influence of street layouts and viaduct settings on daily carbon monoxide exposure and intake fraction in idealized urban canyons, Environ. Pollut. 220 (2017) 72-86.
[3] W. Ji, B. Zhao, Estimating Mortality Derived from Indoor Exposure to Particles of Outdoor Origin, Plos One 10(4) (2015) 15.
[4] C. Gromke, B. Ruck, Pollutant concentrations in street canyons of different aspect ratio with avenues of trees for various wind directions, Bound.-Layer Meteorol. 144(1) (2012) 41-64.
[5] R. Buccolieri, M. Sandberg, S. Di Sabatino, City breathability and its link to pollutant concentration distribution within urban-like geometries, Atmos. Environ. 44(15) (2010) 1894-1903.
[6] J. Hang, Z. Xian, D. Wang, C.M. Mak, B. Wang, Y. Fan, The impacts of viaduct settings and street aspect ratios on personal intake fraction in three-dimensional urban-like geometries, Build. Environ. 143 (2018) 138-162.
[7] Y. Du, C.M. Mak, Z. Ai, Modelling of pedestrian level wind environment on a high-quality mesh: A case study for the HKPolyU campus, Environ. Model. Softw. 103 (2018) 105-119.
[8] Y. Du, C.M. Mak, Y. Li, Application of a multi-variable optimization method to determine lift-up design for optimum wind comfort, Build. Environ. 131 (2018) 242-254.
[9] Y. Du, C.M. Mak, Y. Li, A multi-stage optimization of pedestrian level wind environment and thermal comfort with lift-up design in ideal urban canyons, Sustain. Cities Soc. 46 (2019) 101424.
[10] D. Cui, G. Hu, Z. Ai, Y. Du, C.M. Mak, K. Kwok, Particle image velocimetry measurement and CFD simulation of pedestrian level wind environment around U-type street canyon, Build. Environ. 154 (2019) 239-251.
[11] Y. Du, B. Blocken, S. Pirker, A novel approach to simulate pollutant dispersion in the built environment: Transport-based recurrence CFD, Build. Environ. 170 (2020) 106604.
[12] J. Hang, M. Lin, D.C. Wong, X. Wang, B. Wang, R. Buccolieri, On the influence of viaduct and ground heating on pollutant dispersion in 2D street canyons and toward single-sided ventilated buildings, Atmos. Pollut. Res. 7(5) (2016) 817-832.
[13] T. Michioka, H. Takimoto, H. Ono, A. Sato, Effect of fetch on a mechanism for pollutant removal from a two-dimensional street canyon, Bound.-Layer Meteorol. 160(1) (2016) 185-199.
[14] K. Zhang, G. Chen, X. Wang, S. Liu, C.M. Mak, Y. Fan, J. Hang, Numerical evaluations of urban design technique to reduce vehicular personal intake fraction in deep street canyons, Sci. Total Environ. 653 (2019) 968-994.

[15] Z. Ai, C.M. Mak, Wind-induced single-sided natural ventilation in buildings near a long street canyon: CFD evaluation of street configuration and envelope design, J. Wing. Eng. Ind. Aerod. 172 (2018) 96-106.
[16] P. Nejat, F. Jomehzadeh, H.M. Hussen, J.K. Calautit, A. Majid, M. Zaimi, Application of Wind as a Renewable Energy Source for Passive Cooling through Windcatchers Integrated with Wing Walls, Energies 11(10) (2018) 2536.
[17] S. Tong, N.H. Wong, E. Tan, S.K. Jusuf, Experimental study on the impact of facade design on indoor thermal environment in tropical residential buildings, Build. Environ. 166 (2019) 106418.
[18] A. Aflaki, N. Mahyuddin, Z.A.-C. Mahmoud, M.R. Baharum, A review on natural ventilation applications through building façade components and ventilation openings in tropical climates, Energy Build. 101 (2015) 153-162.
[19] Z. Ai, C.M. Mak, J. Niu, Z. Li, Q. Zhou, The effect of balconies on ventilation performance of low-rise buildings, Indoor Built Environ. 20(6) (2011) 649-660.
[20] J. Park, J.-I. Choi, G.H. Rhee, Enhanced single-sided ventilation with overhang in buildings, Energies 9(3) (2016) 122.
[21] C.M. Mak, J. Niu, C. Lee, K. Chan, A numerical simulation of wing walls using computational fluid dynamics, Energy Build. 39(9) (2007) 995-1002.
[22] F. Murena, B. Mele, Effect of balconies on air quality in deep street canyons, Atmos. Pollut. Res. 7(6) (2016) 1004-1012.
[23] L. He, J. Hang, X. Wang, B. Lin, X. Li, G. Lan, Numerical investigations of flow and passive pollutant exposure in high-rise deep street canyons with various street aspect ratios and viaduct settings, Sci. Total Environ. 584 (2017) 189-206.
[24] G. Habilomatis, A. Chaloulakou, A CFD modeling study in an urban street canyon for ultrafine particles and population exposure: The intake fraction approach, Sci. Total Environ. 530 (2015) 227-232.
[25] Z. Luo, Y. Li, W.W. Nazaroff, Intake fraction of nonreactive motor vehicle exhaust in Hong Kong, Atmos. Environ. 44(15) (2010) 1913-1918.
[26] C. Chau, E. Tu, D. Chan, J. Burnett, Estimating the total exposure to air pollutants for different population age groups in Hong Kong, Environ. Int. 27(8) (2002) 617-630.
[27] X.-X. Li, D.Y. Leung, C.-H. Liu, K.M. Lam, Physical modeling of flow field inside urban street canyons, J.Appl. Meteorol. Clim. 47(7) (2008) 2058-2067.
[28] J. Franke, A. Hellsten, K.H. Schlunzen, B. Carissimo, The COST 732 Best Practice Guideline for CFD simulation of flows in the urban environment: a summary, Int. J. Environ Pollut. 44(1-4) (2011) 419-427.
[29] Y. Tominaga, A. Mochida, R. Yoshie, H. Kataoka, T. Nozu, M. Yoshikawa, T. Shirasawa, AIJ guidelines for practical applications of CFD to pedestrian wind environment around buildings, J. Wind Eng. Ind. Aero. 96(10-11) (2008) 1749-1761.
[30] V. Yakhot, S.A. Orszag, Renormalization group analysis of turbulence. I. Basic theory, J. Sci. Comput. 1(1) (1986) 3-51.
[31] Y. Tominaga, T. Stathopoulos, Numerical simulation of dispersion around an isolated cubic building: comparison of various types of k–ε models, Atmos. Environ. 43(20) (2009) 3200-3210.
[32] W.-W. Li, R.N. Meroney, Gas dispersion near a cubical model building. Part I. Mean concentration measurements, J. Wind Eng. Ind. Aero. 12(1) (1983) 15-33.
[33] B. Blocken, R. Vervoort, T. van Hooff, Reduction of outdoor particulate matter concentrations by local removal in semi-enclosed parking garages: a preliminary case study for Eindhoven city center, J. Wind Eng. Ind. Aero. 159 (2016) 80-98.
[34] C.-H. Liu, C.-T. Ng, C.C. Wong, A theory of ventilation estimate over hypothetical urban areas, J. Hazard. Mater. 296 (2015) 9-16.

[35] X. Xie, C.-H. Liu, D.Y. Leung, Impact of building facades and ground heating on wind flow and pollutant transport in street canyons, Atmos. Environ. 41(39) (2007) 9030-9049.
[36] W.H. Snyder, Guideline for fluid modeling of atmospheric diffusion. Fluid modeling report no. 10, (1981). US EPA, Research Triangle Park, NC.
[37] AS.NZS 1170.2, 2002. Australian/New Zealand Standard, Structural design action Parts 2: wind actions. Standards Australia & Standards New Zealand, Sydney, 2002.